JOC The Journal of Organic Chemistry

Article

Cite This: J. Org. Chem. 2019, 84, 6126−6133

pubs.acs.org/joc

Rational Design and Synthesis of a Metalloproteinase-Activatable Probe for Dual-Modality Imaging of Metastatic Lymph Nodes in Vivo

Ling Yin,[‡,∥] Hao Sun,[⊥] Meng Zhao,[†] Anna Wang,[†] Shanshan Qiu,[†] Yinjia Gao,[†] Jianan Ding,[†] Shun-Jun Ji,[*,‡] Haibin Shi,[*,†] and Mingyuan Gao[†,§]

[†]State Key Laboratory of Radiation Medicine and Protection, School for Radiological and Interdisciplinary Sciences (RAD-X) and Collaborative Innovation Center of Radiation Medicine of Jiangsu Higher Education Institutions and [‡]Key Laboratory of Organic Synthesis of Jiangsu Province, College of Chemistry, Chemical Engineering and Materials Science & Collaborative Innovation Center of Suzhou Nano Science and Technology, Soochow University, Suzhou 215123, P. R. China

[§]Institute of Chemistry, Chinese Academy of Sciences, BeiYiJie 2, Zhong Guan Cun, Beijing 100190, P. R. China

[∥]Department of Chemistry and Chemical Engineering, Jining University, Qufu 273155, P. R. China

[⊥]Department of Nuclear Medicine, The First Affiliated Hospital of Soochow University, Suzhou 215006, P. R. China

Supporting Information

ABSTRACT: Lymphatic metastasis is an important prognostic indicator for cancer progression. It is therefore considerably meaningful to develop molecularly targeted imaging probes for noninvasive and accurate identification of metastatic lymph nodes (MLNs) at early stages of tumor metastasis. Herein, we report a novel matrix metalloproteinase-2 (MMP-2)-activatable probe constructed with a near-infrared dye (Cy5), a quencher (QSY21), and a tumor-targeting peptide cRGD covalently linked through a radionuclide (^{125}I)-labeled peptide substrate for accurate detection of MLNs. Upon cleavage with activated MMP-2, the above probe emitted MMP-2 concentration-dependent near-infrared fluorescence, which allows sensitive and specific visualization of MLNs via both optical and single-photon emission computed tomography imaging techniques. We thus envision that this probe would serve as a useful tool for studying tumor-induced lymphangiogenesis.

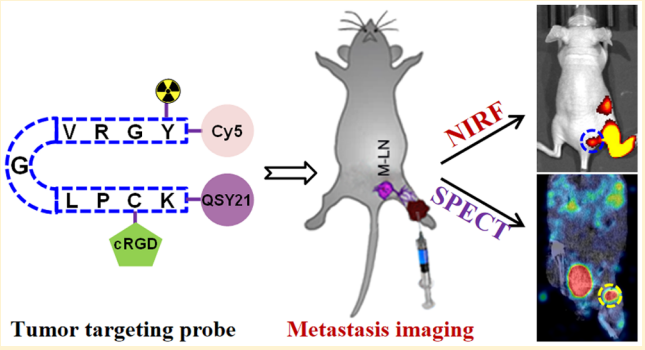

INTRODUCTION

The lymphatic system has currently been recognized as the main route for tumor cell transportation in tumor metastasis. Metastasis to lymph nodes (LNs) represents the first step of tumor dissemination.[1−3] Matrix metalloproteinases (MMPs) have been taken as important biomarkers involved in cancer invasion and metastasis, and MMP-2 belongs to one of the most vital MMPs as it has been demonstrated to be closely associated with lymph node metastasis by mediating the degradation of the extracellular matrix.[4−6] Therefore, it is considerably meaningful to develop an activatable MMP-2-specific probe for noninvasive and accurate identification of metastatic lymph nodes (MLNs) at the early stage of dissemination. Noninvasive detection of protease activity through optical imaging has recently emerged as a powerful tool for both tumor diagnosis and therapeutic evaluation due to its facile and hypersensitive detection of optical signals.[7−15] For example, with the aid of a ratiometric MMP-2-activatable fluorescent probe, accurate and quantitative detection of primary tumors and metastases with increased sensitivity and specificity has been demonstrated, which apparently shows great potential for visualizing the lymph node metastasis.[16,17] Nevertheless, the low signal background ratio and limited penetration depth of visible lights limit their clinical translation. Radioactive nuclear imaging, including positron emission tomography (PET) and single-photon emission computed tomography (SPECT), overcomes the limitations of conventional fluorescence imaging and offers great penetration of tissue with high sensitivity, yet they suffer from low spatial resolution.[18−21] Therefore, multimodality imaging, to combine the advantages of different imaging techniques, has become attractive and promising for tumor metastasis diagnosis.[22,23] Although numerous multimodal nanoprobes, including polymers,[24,25] gold nanoparticles,[26,27] rare-earth-based nanoparticles,[28] mesoporous silica nanoparticles,[29,30] and others,[31−35] have largely been reported for the detection of LNs, the sensitivity and accuracy of MLN detection still need to be further improved. Therefore, it is highly desired to explore new molecular imaging probes with great sensitivity and specificity for MLN detection at early stages of tumor metastasis.

Received: January 31, 2019
Published: April 23, 2019

DOI: 10.1021/acs.joc.9b00331
J. Org. Chem. 2019, 84, 6126−6133

In this study, we report a novel integrin $\alpha_v\beta_3$-targeted and MMP-2-activatable probe that was used for near-infrared fluorescence (NIRF)/SPECT dual-modality imaging of metastatic lymph nodes. As schematically shown in Schemes 1 and 2, a MMP-2-cleavable peptide sequence KCPLGVRGY was chosen to covalently link a near-infrared dye (Cy5), a quencher (QSY21), and a tumor-targeting peptide cRGD to establish a MMP-2-activatable structure QSY21-KC(cRGD)-PLGVRGY-Cy5, which is denoted cRGD-QC below. The probe was further labeled with radionuclide (^{125}I) through the side chain group of tyrosine (Y) to afford the radioactive probe ^{125}I-cRGD-QC for SPECT imaging. The probe in the intact state is optically silent at the beginning, but upon proteolytic cleavage with activated MMP-2, it can result in separation of the QSY21/Cy5 pair and loss of FRET to emit strong near-infrared fluorescence. These features make ^{125}I-cRGD-QC serve as an imaging probe for detecting the MMP-2 activity as well as MMP-2-activated lymph node metastasis in vivo through both NIRF and SPECT imaging techniques.

Scheme 1. Illustration of cRGD-QC for Detection of MMP-2 Activity

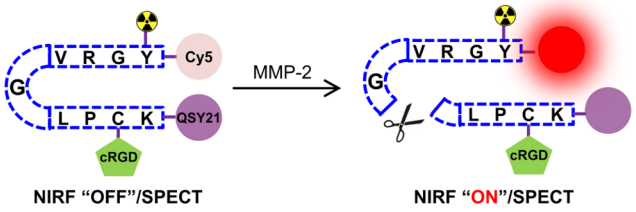

RESULTS AND DISCUSSION

We hypothesized that the introduction of a cRGD moiety would improve the uptake and retention of the probes within metastatic LNs. As a proof of concept, the study began with the synthesis of the targeted probe (cRGD-QC) and the control probe (QC) (Scheme S1). Both probes were synthesized according to our previously reported protocol.[36−38] In brief, an alkyne-terminated peptide KCPLGVRGY was first conjugated to an azido-functionalized Cy5 (Cy5-N_3) in a dimethyl sulfoxide (DMSO)/water (1:1 by vol) mixture by a copper(I)-catalyzed "click" reaction and then reacted with QSY21 NHS (QSY21 carboxylic acid, succinimidyl ester) to afford the control probe QSY21-KCPLGVRGY-Cy5, which is denoted QC below. QC was further conjugated with a maleimide-functionalized cyclic RGD (cRGD-Mal) via the thiol group of cysteine to obtain the desired probe cRGD-QC in 93.6% yield. The purity and identity of both the probes were verified by analytical HPLC and high-resolution mass spectrometry (HRMS) (Figures 1a and S1−S7).

To investigate the responsiveness of the probe to MMP-2, we performed in vitro enzymatic assays with recombinant MMP-2 first. cRGD-QC (4 μM) was incubated with activated MMP-2 (640 ng mL^{-1}) in HEPES buffer (pH = 7.4) at 37 °C for 2 h. As expected, the fluorescence of cRGD-QC was remarkably activated with a 12.8-fold fluorescence enhancement, as given in Figure 1b. However, the activation was effectively blocked by pretreatment of the probe with GM6001, a highly specific inhibitor of MMP-2, suggesting that the current probe possesses excellent specificity in response to MMP-2. HPLC analysis further confirmed that the probe cRGD-QC was clearly digested by activated MMP-2 to generate two fragments (Figure 1a). To further characterize the sensitivity of the probe in detecting MMP-2, cRGD-QC (4 μM) was incubated with MMP-2 with concentrations ranging from 0 to 640 ng mL^{-1} in HEPES buffer (pH = 7.4, 37 °C) for 2 h. As shown in Figures 1c and S8, the fluorescence was progressively intensified and positively correlated with the concentrations of MMP-2. When the concentration of MMP-2 was lower than 320 ng mL^{-1}, the intensity of the activated fluorescence went linearly against the MMP-2 concentration (R^2 = 0.99), according to which a detection limit down to 4.8 ng mL^{-1} can be derived. To assess the selectivity of the probe, cRGD-QC was also treated under the identical conditions with different types of proteins, such as *Bam*HI, bovine serum albumin (BSA), furin, RNase, MMP-9, and MMP-2. The results given in Figure 1d revealed that both MMP-9 and

Scheme 2. Synthesis of Probe ^{125}I-cRGD-QC

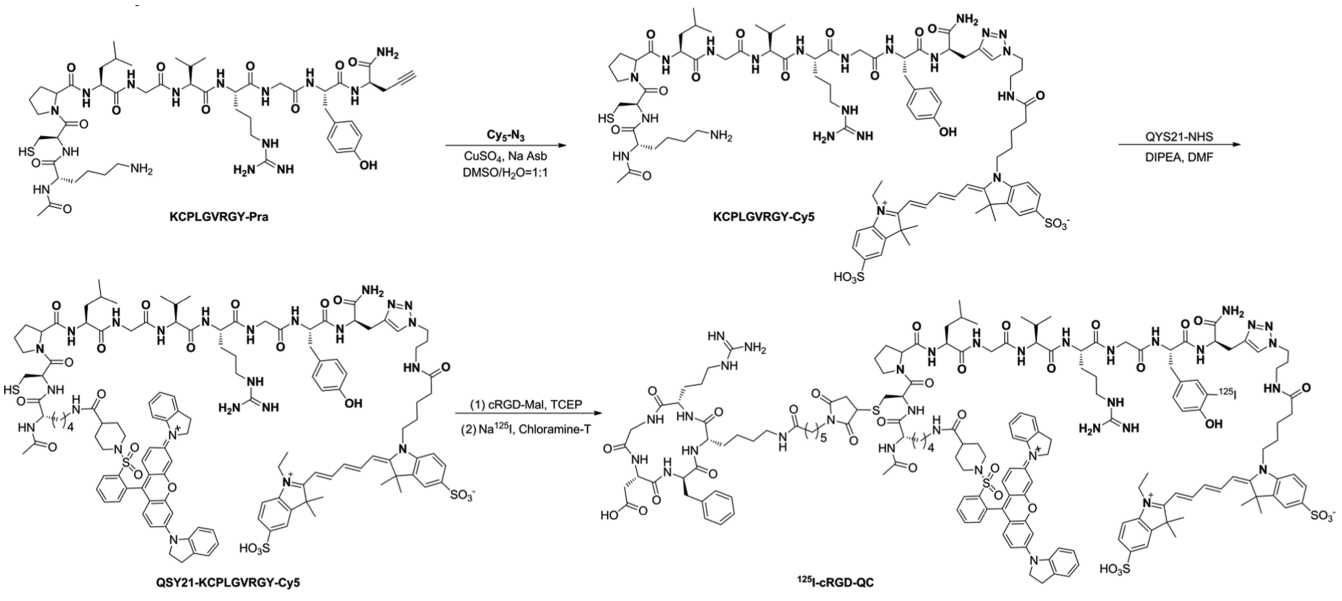

DOI: 10.1021/acs.joc.9b00331
J. Org. Chem. 2019, 84, 6126−6133

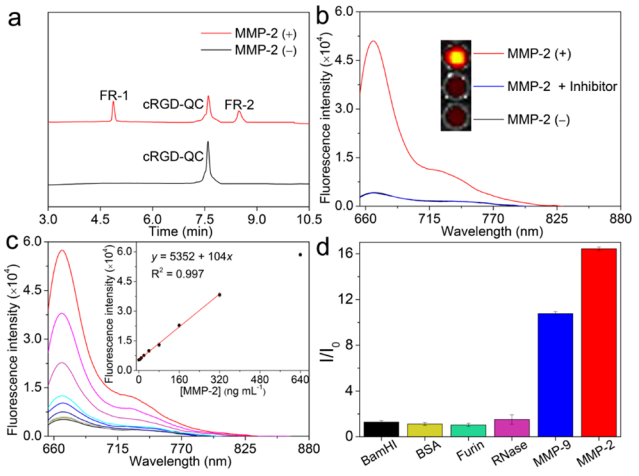

Figure 1. (a) HPLC profile of cRGD-QC (4 μM) determined before (black) and after (red) incubation with MMP-2 (640 ng mL^{-1}) at 37 °C for 2 h. FR-1: Cy5-YGRVG, FR-2: cRGD-QSY21-KCPL. (b) Fluorescence spectra of cRGD-QC (4 μM) recorded after incubation with MMP-2 (640 ng mL^{-1}) [denoted MMP-2(+)], a mixture of MMP-2 and its inhibitor GM6001 (100 μM) [denoted MMP-2 + inhibitor] at 37 °C for 2 h in *N*-(2-hydroxyethyl)piperazine-*N*′-ethanesulfonic acid (HEPES) buffer (pH = 7.4), together with the spectrum of the cRGD-QC probe treated in the absence of MMP-2 [denoted MMP-2 (−)] (inset: fluorescence images of the above solutions recorded upon excitation at 646 nm on an IVIS system). (c) Fluorescence spectra of cRGD-QC (4 μM) recorded after incubation with different concentrations of MMP-2 (0, 5, 10, 20, 40, 80, 160, 320, and 640 ng mL^{-1}) at 37 °C for 2 h (inset: MMP-2 concentration-dependent fluorescence of the cRGD-QC probe). (d) Fluorescence intensity ratio (I/I_0) of the same amount (640 ng mL^{-1}) of different enzymes (*Bam*HI, bovine serum albumin (BSA), furin, RNase, MMP-9 and MMP-2) incubated with cRGD-QC (4 μM) at 37 °C for 2 h. The error bars represent standard deviations (SD) of three separate measurements.

MMP-2 could effectively activate the probe with 10.8- and 16.5-fold fluorescence enhancements, respectively. Collectively, all of these results demonstrate that this probe is indeed a highly sensitive and selective probe for MMP-9/-2.

To explore the potential of the probe for in vitro live-cell imaging of MMP-2, the cytotoxicity of cRGD-QC was first assessed through the widely used methyl thiazolyl tetrazolium (MTT) assay. As shown in Figure S9, the probe exhibited negligible cytotoxicity to murine breast carcinoma 4T1 cells in a concentration range of 0−64 μM after incubation with the cells for 24 h. The overall cell viability remained above 80%. Next, confocal laser scanning microscopy was used to image 4T1 living cells treated with different concentrations of cRGD-QC and QC after 6 h incubation. As shown in Figure 2, the cells treated with cRGD-QC apparently showed stronger fluorescence than the cells receiving QC, suggesting that the cRGD−integrin interaction mediated the increased internalization of the probes. Additionally, with increasing concentrations of the probes used, the cell fluorescence was progressively intensified. Moreover, the fluorescence signals could be remarkably suppressed when the cells were pretreated with the MMP-2 inhibitor before incubation with probes. Collectively, all of the above results demonstrate that the cRGD-QC probe is undoubtedly a specific probe for the detection of MMP-2 activity in cancer cells, which encouraged us to further evaluate its potential for in vivo visualization of MMP-2 activity in metastatic lymph nodes.

The imaging of LNs has been considered to be a valuable method for noninvasive tracking of tumor metastasis in clinics. To further explore the potential of the probe for imaging metastatic LNs in vivo, we developed a mouse model bearing 4T1 murine breast tumor xenografts on its right rear footpad and performed the real-time fluorescence imaging of metastatic LNs with both cRGD-QC and QC. Figure 3a shows a series of representative fluorescence images of mice (n = 3) acquired at selected time points after intradermal injection of the probes

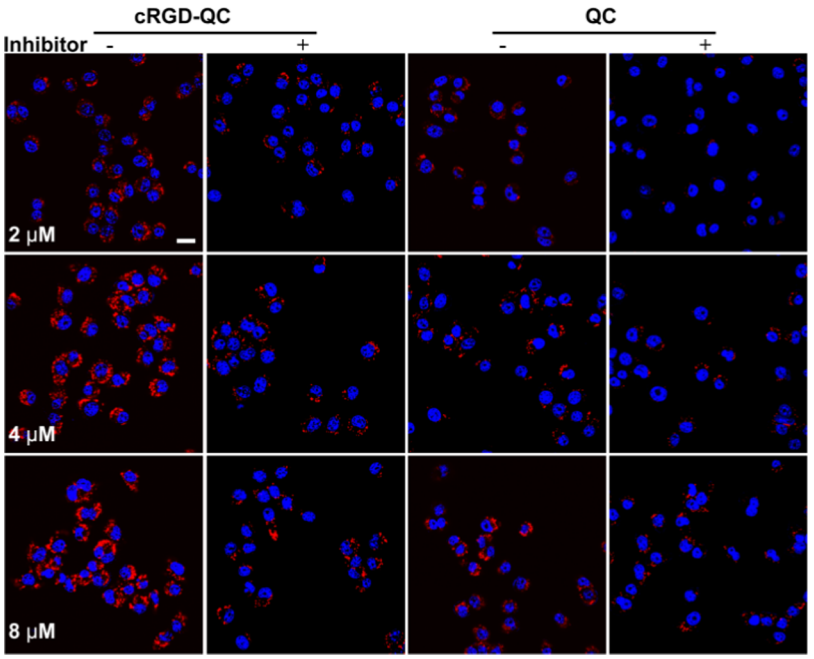

Figure 2. Confocal imaging of mouse breast cancer 4T1 cells after incubation with different concentrations of cRGD-QC and QC (2, 4, and 8 μM) in the presence and absence of inhibitor GM6001 (100 μM). The scale bar indicates 20 μm.

DOI: 10.1021/acs.joc.9b00331
J. Org. Chem. 2019, 84, 6126−6133

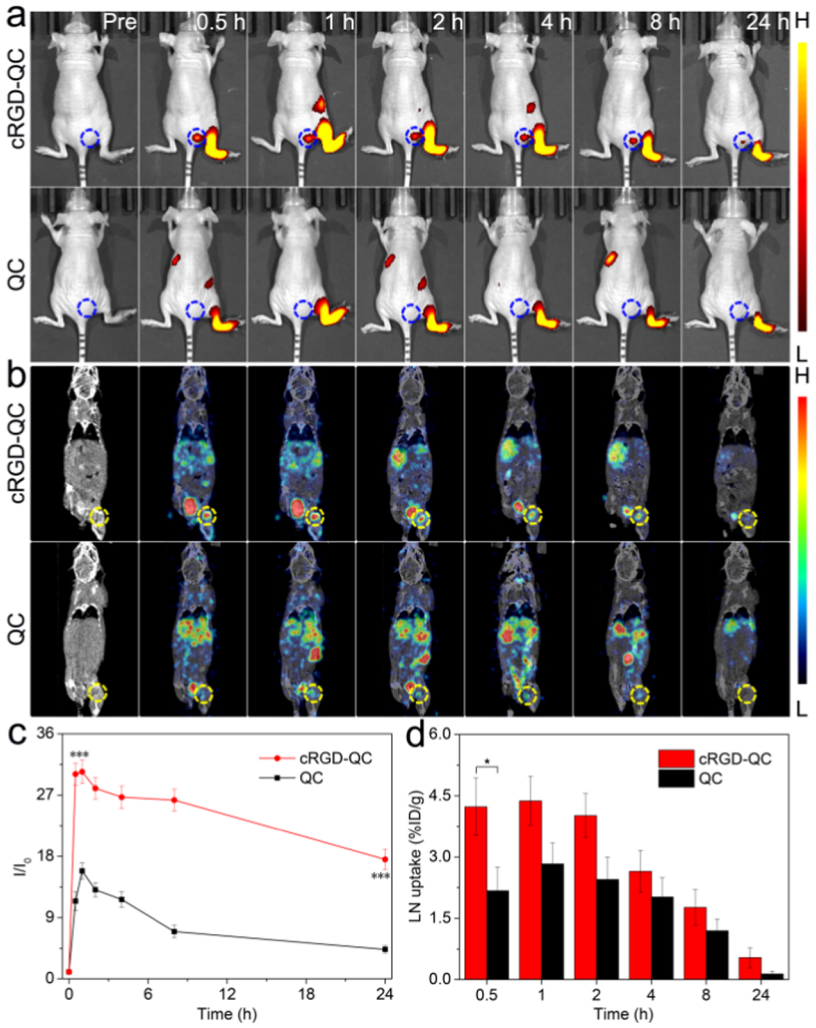

Figure 3. (a) In vivo fluorescence imaging of subcutaneous 4T1 tumor-bearing nude mice at 0.5, 1, 2, 4, 8, and 24 h after injection of cRGD-QC (2 mM, 50 μL) and QC (2 mM, 50 μL) from the right rear footpad. (b) Representative SPECT images acquired at different time points postinjection of ^{125}I-cRGD-QC (200 μCi, 50 μL) and ^{125}I-QC (200 μCi, 50 μL). (c) Fluorescence intensity ratio (I/I_0) recorded from the tumor site of the mice shown in (a). (d) LN uptake at different time points of two different ^{125}I-probes (200 μCi, 50 μL). The error bars represent standard deviations (SD) of three separate measurements. Statistical significance: *p < 0.05, **p < 0.01, and ***p < 0.001. Data are represented as mean ± SD.

into the right paw of mice. Notably, the initial lymphatic vessel drainage and lymph nodes from the inoculated side of mice injected with cRGD-QC (2 mM, 50 μL) were clearly visualized through high signal-to-noise fluorescence from 0.5 to 24 h postinjection. The NIR fluorescence signals of LNs appeared 0.5 h postinjection of the cRGD-QC probe and reached an intensity maximum approximately 1 h postinjection. However, the fluorescence signals from the groups of mice that received QC (2 mM, 50 μL) exhibited greatly lowered fluorescence intensity at all of the time intervals, which is probably due to the poor tumor targeting of QC because of the lack of the cRGD group. The quantitative analysis indicated that the LNs of mice with the treatment of cRGD-QC had 2-fold higher fluorescence signals than the ones with QC at 1 h postinjection (Figure 3c). Interestingly, for both groups of mice, no detectable fluorescence signal was determined from contralateral lymph nodes. Meanwhile, the sizes of the resected LNs from the inoculated side of mice were apparently larger than those from the contralateral side of mice. These results suggest no metastasis to contralateral lymph nodes. Additionally, ex vivo imaging also showed stronger fluorescence signals in the resected LNs of mice receiving cRGD-QC, while weak fluorescence was observed from the MLNs in the mice with the treatment of QC, which is quite consistent with the aforementioned in vivo results shown in Figure 2. The fluorescence intensity ratios (I/I_0) between MLNs and background for both groups of mice were 35 and 16, respectively (Figure S10c). Collectively, these results strongly demonstrate that cRGD-QC has great potential as an NIR probe for sensitive detection of metastatic LNs. Additionally, ex vivo imaging of the excised organs showed that positive fluorescence signals were also determined from the liver region for both groups of mice, indicating that the injected probes entered into blood circulation and were subsequently trapped by the liver (Figure S10a,b). It is noteworthy that QC obviously showed high NIR signals in the liver of mice compared with cRGD-QC, suggesting that cRGD-QC has low uptake in the liver and can effectively accumulate at the tumor region or metastatic LNs.

It is well known that radioactive nuclear imaging, such as SPECT, has recently emerged as one of the most powerful imaging techniques for cancer diagnosis due to its sensitive and quantitative detection of targets. To evaluate the capability of the probes for SPECT imaging of MLNs, both cRGD-QC and

DOI: 10.1021/acs.joc.9b00331
J. Org. Chem. 2019, 84, 6126−6133

QC were labeled with nuclide ^{125}I- and then subcutaneouly injected into the right hind footpads of BALB/c mice bearing 4T1 murine breast tumor xenografts on the right rear paws. Consistent with the aforementioned in vivo NIRF imaging of lymphatic metastasis shown in Figure 3a, the accumulations of both radioactive probes in LNs gradually increased over time (Figure 3b). The radioactivity signals of LNs in the group of mice that received ^{125}I-cRGD-QC (200 μCi, 50 μL) reached an intensity maximum approximately 1 h postinjection with the uptake value of 4.4% ID/g. However, the LNs in the group of mice that received ^{125}I-QC (200 μCi, 50 μL) showed very low radioactivity signals at 1 h postinjection with only 2.8% ID/g uptake (Figure 3d), further confirming the poor tumor targeting of probe QC. As expected, the contralateral lymph nodes in all mice showed weak radioactivity signals. These findings were further corroborated by ex vivo biodistribution data shown in Figure S11b. Collectively, all of these results demonstrate that cRGD-QC exhibits great potential as a dual-modality NIRF/SPECT probe for sensitive identification of metastatic lymph nodes.

In light of the above exciting findings, the specificity of the probe for imaging metastatic LNs was further assessed. 4T1 cells were injected into the right paw of mice to establish the footpad tumor-bearing mice model. Equal amounts of cRGD-QC were intradermally injected in both the left and right hind footpads for normal lymph node (N-LN) and metastatic lymph node (M-LN) imaging. As shown in Figure 4a, time-dependent in vivo NIR fluorescence imaging indicated that M-LNs close to the right inoculated side of mice had obviously strong NIR signals and long imaging time up to 24 h. However, no fluorescence signals were visualized in N-LNs from the left inoculated side of mice all of the time. Region of interest analysis showed that the fluorescence signal ratios between the lymph nodes and background were 83 and 59 for M-LNs and N-LNs, respectively, at 1 h postinjection. The I/I_0 of M-LNs still remained 65 even at 24 h postinjection (Figure 4b). Additionally, the fluorescence and radioactivity signals of lymph nodes were also simultaneously imaged by an ex vivo imaging system, FX Pro. It was found that M-LNs had presented stronger fluorescence and radioactivity signals than N-LNs (Figure S12), which were consistent with the previous in vivo results shown in Figure 4a. All of these pieces of evidence strongly suggest that cRGD-QC can be used for specific detection of metastatic lymph nodes.

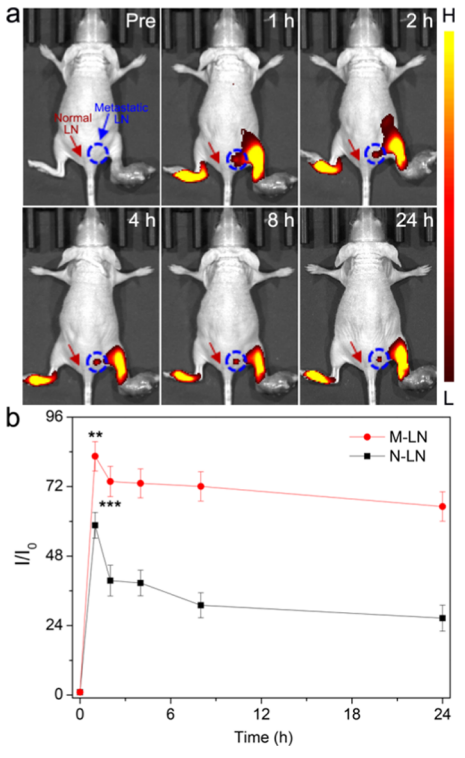

Figure 4. (a) In vivo fluorescence imaging of MLNs in subcutaneous 4T1 tumor-bearing nude mice injected with cRGD-QC (2 mM, 50 μL) from the two sides of rear footpads: M-LN, metastatic lymph node; N-LN, normal lymph node. (b) Fluorescence intensity ratio (I/I_0) recorded from the tumor site of the mice shown in (a). The error bars represent standard deviations (SDs) of three separate measurements. Statistical significance: *p < 0.05, **p < 0.01, and ***p < 0.001. Data are represented as mean ± SD.

CONCLUSIONS

In summary, we have successfully developed an MMP-2-activatable probe cRGD-QC for specific and accurate detection of metastatic lymph nodes. In vivo imaging studies on the 4T1 tumor model have demonstrated the outstanding ability of the probe for detecting the metastatic lymph nodes, owing to its excellent tumor-targeting specificity and imaging sensitivity enabled by the rational NIRF/SPECT dual-modal imaging probe. We thus believe that the current approach may provide a powerful tool for noninvasive and precise diagnosis of lymph node metastasis in vivo.

EXPERIMENTAL SECTION

Materials. *N*-Succinimidyl 6-maleimidohexanoate (EMCS) was provided by Struchem (Suzhou, China). Cy5 azide was obtained from Sigma-Aldrich (St. Louis, MO). c(RGDfK) and KCPLGVRGY-Pra were synthesized by GL Biochem (Shanghai, China) as requested. QSY21 carboxylic acid, succinimidyl ester (QSY21 NHS) was obtained from Molecular Probes (Eugene, OR). Tris(2-carboxyethyl) phosphine hydrochloride (TCEP) was provided by Aladdin (Shanghai, China). MMP-2 and MMP-9 enzymes were obtained from R&D (Minneapolis, MN). RNase was purchased from Thermo Fisher Scientific (Waltham, MA). Furin was obtained from New England Biolabs (Ipswich, MA). *Bam*HI was purchased from Thermo Fisher Scientific (Waltham, MA). BSA was obtained from Sinopharm (Shanghai, China). The MMP inhibitor GM6001 was purchased from TargetMol (Boston, MA). The MTT cell proliferation cytotoxicity assay kit was obtained from Sigma-Aldrich (St. Louis, MO). Hoechst 33342 was purchased from BD (Franklin, NJ). Radionuclide (Na^{125}I) was obtained from GMS Pharmaceutical Co., Ltd (Shanghai, China). All other chemicals were purchased from Sigma-Aldrich (St. Louis, MO). Ultrapure water (18 MΩ cm) was used in the experiments.

Characterization. HRMS was performed on a 6540 UHD accurate-mass quadrupole time-of-flight mass spectrometer (Agilent). HPLC profiles were performed using 1260 high-performance liquid chromatography (Agilent). Fluorescence spectra were recorded using a fluorescence spectrometer (FLS980, Edinburgh). MTT was measured using an EnSpire multimode plate reader (PerkinElmer). The fluorescence micrographs were captured with a fluorescence microscope (FV1200, Olympus). NIR fluorescence and SPECT imaging were recorded using IVIS spectrum (PerkinElmer) and U-SPECT/CT (MILABS), respectively. Fluorescence and radioactivity signals were imaged by an ex vivo imaging system FX Pro (Kodak).

Synthetic Route for cRGD-QC. cRGD-QC was synthesized according to previously reported procedures.[36−38] The synthetic route is shown in Scheme S1.

Synthesis of cRGD-Mal. c(RGDfK) (6.03 mg, 0.01 mmol) and EMCS (6.17 mg, 0.02 mmol) were dissolved in 1 mL of dimethylformamide (DMF), and 30 μL of *N*,*N*-diisopropylethylamine

DOI: 10.1021/acs.joc.9b00331
J. Org. Chem. 2019, 84, 6126−6133

(DIPEA) was slowly dropped into the mixture. The reaction was continued with shaking for about 4 h at room temperature. The final product was purified by prep-HPLC (5.11 mg, 64.1% yield) and further characterized by HRMS. Calcd for $C_{37}H_{53}N_{10}O_{10}^{+}$, ([M + H]$^{+}$): 797.3941, found ESI-MS: m/z 797.3898.

Synthesis of KCPLGVRGY-Cy5. Cy5 azide (3.69 mg, 0.0050 mmol) and KCPLGVRGY-Pra (5.01 mg, 0.0055 mmol) were dissolved in 1 mL of DMSO, and the reaction mixture was shaken for a few minutes to obtain a clear solution. The click reaction was initiated by sequential addition of $CuSO_4$ (0.48 mg, 0.0030 mmol) and sodium ascorbate (1.19 mg, 0.0060 mmol) in 1 mL of H_2O. The reaction was continued with shaking in the dark at room temperature for about 4 h. The final product was purified by prep-HPLC (6.76 mg, 72.4% yield) and further characterized by HRMS. Calcd for $C_{87}H_{129}N_{21}O_{19}S_3^{2+}$, ([M + 2H]$^{2+}$): 933.9462, found ESI-MS: m/z 933.9398.

Synthesis of QC. KCPLGVRGY-Cy5 (2.24 mg, 0.0012 mmol) and QSY21 NHS (0.82 mg, 0.001 mmol) were dissolved in 1 mL of DMF, and then 40 μL of DIPEA was added into the solution. The reaction mixture was stirred for 5 h in the dark at room temperature, monitored by HPLC. The desired products were finally purified by prep-HPLC (2.11 mg, 83.5% yield) and characterized by HRMS. Calcd for $C_{128}H_{163}N_{24}O_{23}S_4^{2+}$, ([M + 2H]$^{2+}$): 1266.0597, found ESI-MS: m/z 1266.0525.

Synthesis of cRGD-QC. To the solution of TCEP (0.50 mg, 0.002 mmol) in 200 μL of Tris buffer (pH = 7.2), cRGD-Mal (3.98 mg, 0.005 mmol) and QC (2.53 mg, 0.001 mmol) were added with stirring for about 3 h in the dark at room temperature, monitored by HPLC. The desired products were finally purified by prep-HPLC (2.89 mg, 86.9% yield) and characterized by HRMS. Calcd for $C_{165}H_{213}N_{34}Na_2O_{33}S_4^{2+}$, ([M + 2Na]$^{2+}$): 1686.2351, found ESI-MS: m/z 1686.0580.

Enzymatic Assays. In vitro enzymatic assays were performed in HEPES buffer (pH = 7.4). Briefly, cRGD-QC (4 μM) was incubated with 0, 5, 10, 20, 40, 80, 160, 320, and 640 ng mL^{-1} recombinant MMP-2 at 37 °C for 2 h in Eppendorf tubes, respectively. Furthermore, MMP-2 (640 ng mL^{-1}) was incubated with cRGD-QC (4 μM) at 37 °C for 2 h. The enzymatic cleavage of the probe by MMP-2 was monitored by HPLC. The fluorescence intensity was measured with an FLS980 spectrometer. The excitation wavelength was fixed at 646 nm, and the emission spectrum was recorded from 655 to 900 nm using a 300 μL cuvette.

For competitive experiments, the MMP-2 inhibitor (GM6001, 100 μM) was first incubated with MMP-2 (640 ng mL^{-1}) for 0.5 h followed by the addition of the probe (4 μM). Meanwhile, the same amount of the probe was directly added into the HEPES solution containing 640 ng mL^{-1} MMP-2. After 2 h incubation at 37 °C, the fluorescence intensity was then recorded with an FLS980 spectrometer.

To investigate the selectivity of the probe, 4 μM probe was incubated with 640 ng mL^{-1} enzymes (*Bam*HI, BSA, furin, RNase, MMP-9, MMP-2) at 37 °C for 2 h, respectively. The fluorescence intensity was subsequently determined with an FLS980 spectrometer. In addition, the fluorescence imaging performed using IVIS spectrum agreed with the fluorescence spectrum.

Cell Culture. The murine breast carcinoma cell line 4T1 was acquired from the Cell Bank of the Chinese Academy of Sciences. The 4T1 cells were cultured in RPMI 1640 medium (Hyclone Inc.), supplemented with 10% fetal bovine serum (Hyclone Inc.) and 1% penicillin streptomycin (Beyotime Inc.) at 37 °C in a humidified atmosphere of 5% CO_2. The cells were cultured until 75% confluence was reached, and experiments were performed.

Cytotoxicity Assay of the Probe. The cytotoxicity of the probe was measured using the common MTT assay. 4T1 cells were planted at a density of 1 × 10^4 cells per well in a 96-well cell culture plate. After growing for 24 h, the cells were incubated with different concentrations of cRGD-QC (0, 2, 4, 8, 16, 32, and 64 μM). Then, the cell viability was determined by an MTT cell proliferation cytotoxicity assay kit 24 h after the treatment. The absorbance was measured using an EnSpire multimode plate reader at a wavelength of 490 nm.

Confocal Imaging of the Probe. The 4T1 cells were planted in an 8-well plate with a concentration of 1 × 10^4 cells per well. After growing for 24 h, the cells were incubated with different concentrations of QC (2, 4, and 8 μM) and cRGD-QC (2, 4, and 8 μM) for 6 h at 37 °C. At the same time, the cells were incubated with the probe in the presence of the inhibitor GM6001 (100 μM). The cells were then treated with a Hoechst 33342 assay kit. Fluorescence imaging was then acquired through an FV1200 laser scanning confocal microscope.

Mice Tumor Model. All animal experiments were approved by the Animal Ethics Committee of Soochow University (Suzhou, China). The 4-week-old female BALB/c athymic nude mice with body weights of 18−20 g were purchased from Chang Zhou Cavensla Experimental Animal Technology Co. Ltd. The mice were housed under standard conditions (25 ± 2 °C/60 ± 10% relative humidity) with a 12 h light/dark cycle. The tumors were grafted by injection of 1 × 10^6 4T1 cells in 25 μL of phosphate-buffered saline (PBS) into the right rear footpad of each mouse. Fluorescence and SPECT studies were carried out when the tumor size reached about 50 mm^3.

In Vivo Fluorescence Imaging of Tumors. For NIRF imaging, mice were first anesthetized with 3% isoflurane mixed with oxygen gas (0.5 L min^{-1}). Subsequently, QC (2 mM, 50 μL) and cRGD-QC (2 mM, 50 μL) were subcutaneously injected into the right rear footpad of the mice manifesting lymph node metastases. There are two groups of mice (three mice per group). In addition, cRGD-QC (2 mM, 50 μL) was intratumorally injected into the two sides of the rear footpad of each mouse (n = 3). Fluorescence imaging was recorded on IVIS spectrum at different time points. The fluorescence images were finally analyzed with vendor software to separate autofluorescence from chromophore signals through spectral unmixing algorithms.

Ex Vivo Biodistribution Studies. For the ex vivo biodistribution study, mice were sacrificed at 24 h postinjection of QC (2 mM, 50 μL) and cRGD-QC (2 mM, 50 μL). The major organs and lymph nodes were carefully harvested and rinsed with PBS buffer (pH = 7.4), placed on black paper, and immediately imaged with IVIS spectrum.

Radioiodination of the Probe with the Chloramine-T Method. The probes were labeled with ^{125}I using the chloramine-T method.[21] First, the probes (400 μg) were dissolved in 200 μL of PBS buffer (0.1 M, pH = 7.4) and labeled with about 37 MBq Na^{125}I (1 mCi). Then, 100 μg of chloramine-T in 10 μL of PBS (0.1 M, pH = 7.4) was added. The reaction mixture was incubated for 10 min with shaking at room temperature. The crude reaction was then passed over a SepPak-C18 column (previously activated with 5 mL of EtOH and 5 mL of 0.1 M PBS), hydrophilic impurities (free iodine-125) were eluted with 5 mL of PBS, and the ^{125}I-probe was eluted with 1 mL of EtOH. After that, the ^{125}I-probe was heated to 40 °C for 10 h with shaking to evaporate EtOH.

In Vivo SPECT Imaging. ^{125}I-QC (2 mM, 50 μL) and ^{125}I-cRGD-QC (2 mM, 50 μL) were intratumorally injected into the right rear footpad of each mouse. SPECT imaging was performed under general anesthesia by inhalation of 3% isoflurane mixed with oxygen gas (0.5 L min^{-1}). The mice were maintained in a prone position on a heated animal bed at 37 °C. The representative SPECT images acquired at different time points, i.e., 0.5, 1, 2, 4, 8, and 24 h postinjection of the ^{125}I-probe. The projection data were reconstructed with U-SPECT/CT. After SPECT data reconstruction, the images were analyzed using PMOD software (PMOD Technologies). The experiment was repeated three times for each group.

Biodistribution Study. ^{125}I-QC (2 mM, 25 μL) and ^{125}I-cRGD-QC (2 mM, 25 μL) were intratumorally injected into the right rear footpad of each mouse. There are two groups of mice (three mice per group). The mice were sacrificed at 4 h postinjection, and the major organs and lymph nodes were carefully harvested and weighed. The radioactivity uptakes of the ^{125}I-probe in the various organs were measured in a γ-counter.

Lymph Node Metastasis Imaging. ^{125}I-QC (2 mM, 50 μL) and ^{125}I-cRGD-QC (2 mM, 50 μL) were injected into primary tumors at the right rear footpad of each mouse, respectively. The lymph nodes

DOI: 10.1021/acs.joc.9b00331
J. Org. Chem. 2019, 84, 6126−6133

were harvested at 1 h postinjection, the fluorescence and radioactivity signals were imaged by the ex vivo imaging system FX Pro.

■ ASSOCIATED CONTENT

Supporting Information

The Supporting Information is available free of charge on the ACS Publications website at DOI: 10.1021/acs.joc.9b00331.

Synthetic route of QSY21-KC(cRGD)-PLGVRGY-Cy5 (cRGD-QC); HRMS spectra of cRGD-Mal, KCPLGVRGY-Cy5, QSY21-KCPLGVRGY-Cy5 (QC), and QSY21-KC(cRGD)-PLGVRGY-Cy5 (cRGD-QC); fluorescence images of cRGD-QC treated with different concentrations of MMP-2 using IVIS spectrum; cytotoxicity assays of different concentrations of cRGD-QC measured using MTT with mouse breast cancer 4T1 cells; fluorescence image and intensity of dissected organs of subcutaneous 4T1 tumor-bearing nude mice executed at 24 h after injection of cRGD-QC and QC from the right rear footpad; representative SPECT images acquired at different time points postinjection of ^{125}I-cRGD-QC and ^{125}I-QC; tissue uptake of ^{125}I in the various organs calculated at 4 h postinjection of two different ^{125}I-probes; fluorescence and radioactivity signals and intensity of the lymph nodes of 4T1 tumor-bearing nude mice postinjection of ^{125}I-cRGD-QC and ^{125}I-QC (PDF)

■ AUTHOR INFORMATION

Corresponding Authors

*E-mail: Shunjun@suda.edu.cn (S.-J.J.).
*E-mail: hbshi@suda.edu.cn (H.S.).

ORCID

Shun-Jun Ji: 0000-0002-4299-3528
Haibin Shi: 0000-0003-2234-9126
Mingyuan Gao: 0000-0002-7360-3684

Notes

The authors declare no competing financial interest.

■ ACKNOWLEDGMENTS

We acknowledge the financial support from the National Key Research and Development Program of China (2016YFC0101200, 2018YFA0208800), National Natural Science Foundation of China (21572153), the Key Research and Development Program of Social Development of Jiangsu Province (BE2018655), the Key Program of Natural Science Foundation of Jiangsu Educational Committee (15KJA310004), the Open Project Program of Jiangsu Provincial Key Laboratory of Radiation Medicine and Protection (KJS1767), a Project Funded by the Priority Academic Program Development of Jiangsu Higher Education Institutions, and the Talent Culturing Plan for Leading Disciplines of University of Shandong Province.

■ REFERENCES

(1) Morton, D. L.; Chan, A. D. The concept of sentinel node localization: how it started. *Semin. Nucl. Med.* **2000**, *30*, 4−10.
(2) Detmar, M.; Hirakawa, S. The formation of lymphatic vessels and its importance in the setting of malignancy. *J. Exp. Med.* **2002**, *196*, 713−718.
(3) Alitalo, A.; Detmar, M. Interaction of tumor cells and lymphatic vessels in cancer progression. *Oncogene* **2012**, *31*, 4499−4508.
(4) Egeblad, M.; Werb, Z. New functions for the matrix metalloproteinases in cancer progression. *Nat. Rev. Cancer* **2002**, *2*, 161−174.
(5) Savariar, E. N.; Felsen, C. N.; Nashi, N.; Jiang, T.; Ellies, L. G.; Steinbach, P.; Tsien, R. Y.; Nguyen, Q. T. Real-time in vivo molecular detection of primary tumors and metastases with ratiometric activatable cell-penetrating peptides. *Cancer Res.* **2013**, *73*, 855−864.
(6) Wu, Z. Y.; Li, J. H.; Zhan, W. H.; He, Y. L. Lymph node micrometastasis and its correlation with MMP-2 expression in gastric carcinoma. *World J. Gastroenterol.* **2006**, *12*, 2941−2944.
(7) Zhang, Y.; So, M. K.; Rao, J. Protease-modulated cellular uptake of quantum dots. *Nano Lett.* **2006**, *6*, 1988−1992.
(8) (a) Lee, S.; Cha, E. J.; Park, K.; Lee, S. Y.; Hong, J. K.; Sun, I. C.; Kim, S. Y.; Choi, K.; Kwon, I. C.; Kim, K.; Ahn, C. H. A near-infrared-fluorescence-quenched gold-nanoparticle imaging probe for in vivo drug screening and protease activity determination. *Angew. Chem., Int. Ed.* **2008**, *47*, 2804−2807. (b) Yin, L.; Sun, H.; Zhang, H.; He, L.; Qiu, L.; Lin, J. G.; Xia, H. W.; Zhang, Y. Q.; Ji, S. J.; Shi, H. B.; Gao, M. Y. Quantitatively visualizing tumor-related protease activity in vivo using a ratiometric photoacoustic probe. *J. Am. Chem. Soc.* **2019**, *141*, 3265−3273.
(9) Lee, S.; Ryu, J. H.; Park, K.; Lee, A.; Lee, S. Y.; Youn, I. C.; Ahn, C. H.; Yoon, S. M.; Myung, S. J.; Moon, D. H.; Chen, X.; Choi, K.; Kwon, I. C.; Kim, K. Polymeric nanoparticle-based activatable near-infrared nanosensor for protease determination in vivo. *Nano Lett.* **2009**, *9*, 4412−4416.
(10) Myochin, T.; Hanaoka, K.; Iwaki, S.; Ueno, T.; Komatsu, T.; Terai, T.; Nagano, T.; Urano, Y. Development of a series of near-infrared dark quenchers based on Si-rhodamines and their application to fluorescent probes. *J. Am. Chem. Soc.* **2015**, *137*, 4759−4765.
(11) Blum, G.; von Degenfeld, G.; Merchant, M. J.; Blau, H. M.; Bogyo, M. Noninvasive optical imaging of cysteine protease activity using fluorescently quenched activity-based probes. *Nat. Chem. Biol.* **2007**, *3*, 668−677.
(12) Huang, C. W.; Li, Z.; Conti, P. S. Radioactive smart probe for potential corrected matrix metalloproteinase imaging. *Bioconjugate Chem.* **2012**, *23*, 2159−2167.
(13) Ryu, J. H.; Lee, A.; Lee, S.; Ahn, C. H.; Park, J. W.; Leary, J. F.; Park, S.; Kim, K.; Kwon, I. C.; Youn, I. C.; Choi, K. "One-step" detection of matrix metalloproteinase activity using a fluorogenic peptide probe-immobilized diagnostic kit. *Bioconjugate Chem.* **2010**, *21*, 1378−1384.
(14) Lee, S.; Xie, J.; Chen, X. Activatable molecular probes for cancer imaging. *Curr. Top. Med. Chem.* **2010**, *10*, 1135−1144.
(15) (a) Weissleder, R.; Tung, C. H.; Mahmood, U.; Bogdanov, A. In vivo imaging of tumors with protease-activated near-infrared fluorescent probes. *Nat. Biotechnol.* **1999**, *17*, 375−378. (b) Li, J. C.; Pu, K. Y. Development of organic semiconducting materials for deep-tissue optical imaging, phototherapy and photoactivation. *Chem. Soc. Rev.* **2019**, *48*, 38−71. (c) Zhang, J. J.; Zhen, X.; Upputuri, P. K.; Pramanik, M.; Chen, P.; Pu, K. Y. Activatable photoacoustic nanoprobes for in vivo ratiometric imaging of peroxynitrite. *Adv. Mater.* **2017**, *29*, No. 1604764. (d) Miao, Q.; Yeo, D. C.; Wiraja, C.; Zhang, J. J.; Ning, X. Y.; Xu, C. J.; Pu, K. Y. Near-infrared fluorescent molecular probe for sensitive imaging of keloid. *Angew. Chem., Int. Ed.* **2018**, *57*, 1256−1260.
(16) Ma, T. C.; Hou, Y.; Zeng, J. F.; Liu, C. Y.; Zhang, P. S.; Jing, L. H.; Shangguan, D. H.; Gao, M. Y. Dual-ratiometric target-triggered fluorescent probe for simultaneous quantitative visualization of tumor microenvironment protease activity and pH in vivo. *J. Am. Chem. Soc.* **2018**, *140*, 211−218.
(17) Hou, Y.; Zhou, J.; Gao, Z. Y.; Sun, X. Y.; Liu, C. Y.; Shangguan, D. H.; Yang, W.; Gao, M. Y. Protease-activated ratiometric fluorescent probe for pH mapping of malignant tumors. *ACS Nano* **2015**, *9*, 3199−3205.
(18) Ametamey, S. M.; Honer, M.; Schubiger, P. A. Molecular imaging with PET. *Chem. Rev.* **2008**, *108*, 1501−1516.
(19) (a) Stockhofe, K.; Postema, J. M.; Schieferstein, H.; Ross, T. L. Radiolabeling of nanoparticles and polymers for PET imaging.

DOI: 10.1021/acs.joc.9b00331
J. Org. Chem. 2019, 84, 6126−6133

Pharmaceuticals **2014**, *7*, 392−418. (b) Beer, A. J.; Niemeyer, M.; Carlsen, J.; Sarbia, M.; Nahrig, J.; Watzlowik, P.; Wester, H.-J.; Harbeck, N.; Schwaiger, M. Patterns of $\alpha v\beta 3$ expression in primary and metastatic human breast cancer as shown by ^{18}F-Galacto-RGD PET. *J. Nucl. Med.* **2008**, *49*, 255−259.

(20) Bao, X.; Wang, M. W.; Luo, J. M.; Wang, S. Y.; Zhang, Y. P.; Zhang, Y. J. Optimization of early response monitoring and prediction of cancer antiangiogenesis therapy via noninvasive PET molecular imaging strategies of multifactorial bioparameters. *Theranostics* **2016**, *6*, 2084−2098.

(21) Chen, L.; Chen, J.; Qiu, S.; Wen, L.; Wu, Y.; Hou, Y.; Wang, Y.; Zeng, J.; Feng, Y.; Li, Z.; Shan, H.; Gao, M. Biodegradable nanoagents with short biological half-Life for SPECT/PAI/MRI multimodality imaging and PTT therapy of tumors. *Small* **2018**, *14*, No. 1702700.

(22) Heinzmann, K.; Carter, L. M.; Lewis, J. S.; Aboagye, E. O. Multiplexed imaging for diagnosis and therapy. *Nat. Biomed. Eng.* **2017**, *1*, 697−713.

(23) Pu, K.; Shuhendler, A. J.; Jokerst, J. V.; Mei, J. G.; Gambhir, S. S.; Bao, Z. N.; Rao, J. H. Semiconducting polymer nanoparticles as photoacoustic molecular imaging probes in living mice. *Nat. Nanotechnol.* **2014**, *9*, 233−239.

(24) (a) Noh, Y. W.; Kong, S. H.; Choi, D. Y.; Park, H. S.; Yang, H. K.; Lee, H. J.; Kim, H. C.; Kang, K. W.; Sung, M. H.; Lim, Y. T. Near-infrared emitting polymer nanogels for efficient sentinel lymph node mapping. *ACS Nano* **2012**, *6*, 7820−7831. (b) Jiang, Y. Y.; Pu, K. Y. Multimodal biophotonics of semiconducting polymer nanoparticles. *Acc. Chem. Res.* **2018**, *51*, 1840−1849.

(25) (a) Lyu, Y.; Xie, C.; Chechetka, S. A.; Miyako, E.; Pu, K. Y. Semiconducting polymer nanobioconjugates for targeted photothermal activation of neurons. *J. Am. Chem. Soc.* **2016**, *138*, 9049−9052. (b) Li, J. C.; Zhen, X.; Lyu, Y.; Jiang, Y. Y.; Huang, J. G.; Pu, K. Y. Cell-membrane coated semiconducting polymer nanoparticles for enhanced multimodal cancer phototheranostics. *ACS Nano* **2018**, *12*, 8520−8530.

(26) (a) Song, K. H.; Kim, C.; Cobley, C. M.; Xia, Y.; Wang, L. V. Near-infrared gold nanocages as a new class of tracers for photoacoustic sentinel lymph node mapping on a rat model. *Nano Lett.* **2009**, *9*, 183−188. (b) Cheng, X. J.; Sun, R.; Yin, L.; Chai, Z. F.; Shi, H.; Gao, M. Y. Light-triggered assembly of gold nanoparticles for photothermal therapy and photoacoustic imaging of tumors in vivo. *Adv. Mater.* **2017**, *29*, No. 1604894.

(27) Jung, Y.; Reif, R.; Zeng, Y.; Wang, R. K. Three-dimensional high resolution imaging of gold nanorods uptake in sentinel lymph nodes. *Nano Lett.* **2011**, *11*, 2938−2943.

(28) Sun, Y.; Yu, M.; Liang, S.; Zhang, Y.; Li, C.; Mou, T.; Yang, W.; Zhang, X.; Li, B.; Huang, C.; Li, F. Fluorine-18 labeled rare-earth nanoparticles for positron emission tomography (PET) imaging of sentinel lymph node. *Biomaterials* **2011**, *32*, 2999−3007.

(29) Huang, X.; Zhang, F.; Lee, S.; Swierczewska, M.; Kiesewetter, D. O.; Lang, L.; Zhang, G.; Zhu, L.; Gao, H.; Choi, H. S.; Niu, G.; Chen, X. Long-term multimodal imaging of tumor draining sentinel lymph nodes using mesoporous silica-based nanoprobes. *Biomaterials* **2012**, *33*, 4370−4378.

(30) (a) Liu, Z.; Rong, P.; Yu, L.; Zhang, X.; Yang, C.; Guo, F.; Zhao, Y.; Zhou, K.; Wang, W.; Zeng, W. Dual-modality noninvasive mapping of sentinel lymph node by photoacoustic and near-infrared fluorescent imaging using dye-loaded mesoporous silica nanoparticles. *Mol. Pharm.* **2015**, *12*, 3119−3128. (b) Sun, R.; Yin, L.; Zhang, S. H.; He, L.; Cheng, X. J.; Wang, A. N.; Xia, H. W.; Shi, H. B. Simple light-triggered fluorescent labeling of silica nanoparticles for cellular imaging applications. *Chem. - Eur. J.* **2017**, *23*, 13893−13896.

(31) (a) Ting, R.; Aguilera, T. A.; Crisp, J. L.; Hall, D. J.; Eckelman, W. C.; Vera, D. R.; Tsien, R. Y. Fast ^{18}F labeling of a near-infrared fluorophore enables positron emission tomography and optical imaging of sentinel lymph nodes. *Bioconjugate Chem.* **2010**, *21*, 1811−1819. (b) Huang, H.; Lovell, J. F. Advanced functional nanomaterials for theranostics. *Adv. Funct. Mater.* **2017**, *27*, No. 1603524.

(32) (a) Cheng, L.; Yang, K.; Li, Y.; Chen, J.; Wang, C.; Shao, M.; Lee, S. T.; Liu, Z. Facile preparation of multifunctional upconversion nanoprobes for multimodal imaging and dual-targeted photothermal therapy. *Angew. Chem., Int. Ed.* **2011**, *50*, 7385−7390. (b) Beer, A. J.; Niemeyer, M.; Carlsen, J.; Sarbia, M.; Nahrig, J.; Watzlowik, P.; Wester, H. J.; Harbeck, N.; Schwaiger, M. Patterns of alphavbeta3 expression in primary and metastatic human breast cancer as shown by ^{18}F-Galacto-RGD PET. *J. Nucl. Med.* **2008**, *49*, 255−259.

(33) Morais, M.; Campello, M. P.; Xavier, C.; Heemskerk, J.; Correia, J. D.; Lahoutte, T.; Caveliers, V.; Hernot, S.; Santos, I. Radiolabeled mannosylated dextran derivatives bearing an NIR-fluorophore for sentinel lymph node imaging. *Bioconjugate Chem.* **2014**, *25*, 1963−1970.

(34) Qiao, R.; Liu, C.; Liu, M.; Hu, H.; Liu, C.; Hou, Y.; Wu, K.; Lin, Y.; Liang, J.; Gao, M. Ultrasensitive in vivo detection of primary gastric tumor and lymphatic metastasis using upconversion nanoparticles. *ACS Nano* **2015**, *9*, 2120−2129.

(35) (a) Xu, Z.; Wang, Y.; Han, J.; Xu, Q.; Ren, J.; Xu, J.; Wang, Y.; Chai, Z. Noninvasive multimodal imaging of osteosarcoma and lymph nodes using a ^{99m}Tc-labeled biomineralization nanoprobe. *Anal. Chem.* **2018**, *90*, 4529−4534. (b) Wang, A. N.; Yin, L.; He, L.; Xia, H. W.; Chen, F.; Zhao, M.; Ding, J. N.; Shi, H. B. An acidic pH/reduction dual-stimuli responsive nanoprobe for enhanced CT imaging of tumours in vivo. *Nanoscale* **2018**, *10*, 20126−20130.

(36) Shi, H.; Kwok, R. T. K.; Liu, J.; Xing, B.; Tang, B. Z.; Liu, B. Real-time monitoring of cell apoptosis and drug screening using fluorescent light-up probe with aggregation-induced emission characteristics. *J. Am. Chem. Soc.* **2012**, *134*, 17972−17981.

(37) Yu, Z. H.; Luan, F. J.; Leng, X.; Shi, Y. X.; Wang, J.; Yin, L.; He, L.; Shi, H. B.; Chen, W. C. A fluorogenic probe for sensitive detection of MMP-2/9 activities in clinical colorectal cancer tissues. *Chin. Sci. Bull.* **2018**, *63*, 318−326.

(38) Luan, F. J.; Yu, Z. H.; Yin, L.; Leng, X.; Shi, Y. X.; Wang, J.; Shi, H. B.; Chen, W. C. Accurate detection of matrix metalloproteinase-2 activity in clinical gastric cancer tissues using a fluorescent probe. *Anal. Methods* **2019**, *11*, 1516−1521.

DOI: 10.1021/acs.joc.9b00331
J. Org. Chem. 2019, 84, 6126−6133